solar

MDPI

Article

Blueberries as a Source of Energy: Physical Chemistry Characterization of Their Anthocyanins as Dye-Sensitized Solar Cells' Sensitizers

Tatiana Montagni [1], Mauricio Rodríguez Chialanza [2] and María Fernanda Cerdá [1,*]

[1] Laboratorio de Biomateriales, Instituto de Química Biológica, Facultad de Ciencias, UdelaR. Iguá 4225, Montevideo 11400, Uruguay; tmontagni@fcien.edu.uy
[2] PDU Ciencias Física y sus Aplicaciones, Centro Universitario Regional del Este, UdelaR. Ruta 15 y Ruta 9, Rocha 2700, Uruguay; mrodriguez@cure.edu.uy
* Correspondence: fcerda@fcien.edu.uy

Abstract: This work aimed to show the possibility of applying anthocyanins extracted from blueberries following a straightforward path as potential impregnation dyes in dye-sensitized solar cells (DSSCs), particularly in the presence of co-adsorbents, such as silver nanoparticles, as an alternative in order to profit from large amounts of discarded fruits. Following a simple procedure, anthocyanins (mainly delphinidin-3-glucoside) were obtained from blueberries (Southern Highbush type). Complete characterization was carried out in order to prove the utility of delphinidin-3-glucoside as a sensitizer in DSSCs. The analyzed anthocyanin is suitable for sensitizing because of its high molar absorptivity values within the visible region of the light spectra, the adsorption ability to a FTO/TiO_2 electrode (FTO, fluorine-doped tin oxide) as confirmed by Fourier transform infrared (FTIR) as well as thermogravimetry coupled to differential scanning calorimetry (TG-DSC), a potential oxidation value near 1 V, and adequate thermal as well as light stabilities. Moreover, the cell's conversion efficiency is improved in the presence of silver nanoparticles, reaching 0.24% (nearly a 25% increase). The sum of all these characteristics points to the application of delphinidin-3-glucoside as a sensitizer in DSSCs, offering a technological use with potential interest for countries where agricultural production offers an abundant origin of extraction.

Keywords: delphinidin; impedance; DSSC; nanoparticles

Citation: Montagni, T.; Rodríguez Chialanz, M.; Cerdá, M.F. Blueberries as a Source of Energy: Physical Chemistry Characterization of Their Anthocyanins as Dye-Sensitized Solar Cells' Sensitizers. *Solar* **2023**, *3*, 283–297. https://doi.org/10.3390/solar3020017

Academic Editor: Jürgen Heinz Werner

Received: 10 March 2023
Revised: 11 May 2023
Accepted: 15 May 2023
Published: 18 May 2023

1. Introduction

Dye-sensitized solar cells (DSSCs) are based on transparent and colorful materials. They provide an alternative to silicon-based devices for indoor applications and BIPVs (building-integrated photovoltaics) due to their transparency and beauty or for long-term wireless power for Internet of things (IoT) devices and wireless sensors (where the need for current or voltage is low) [1–7]. Dyes can be extracted from natural sources or obtained from synthetic paths, and reach conversion efficiency depending on their origin.

First reported in 1991, DSSCs described power conversion efficiency (PCE) values improved to 13.5% under standard 1 sun, AM 1.5 solar radiations. The documented record is a PCE of 34.5% under ambient light [8–11].

The total efficiency of DSSCs depends strongly on the photoanode composition, where the dye plays a vital role in the transfer processes [12]. Strong dye adsorption onto the TiO_2 is required for efficient electron injection from the pigment to the semiconductor. The selection of photosensitizers in dye-sensitized cells is based on the high molar absorptivity of visible light at different wavelengths, the stability towards the temperature or light, and the costs associated with them being obtained. Among the evaluated sensitizers, several dyes extracted from natural resources (anthocyanins, carotenoids, flavonoids, and chlorophyll) have been reported and represent an attractive alternative regarding their

abundance, costs, and eco-friendly characteristics [13–18]. Conversion efficiencies for natural pigments are much lower than those obtained for synthesized dyes, but they still constitute a research focus [19–26]. Although DSSCs based on synthetic dyes are more efficient, their use of expensive metals, such as N3 and N719, has several drawbacks [27]. DSSCs based on natural dyes could offer an exciting alternative to profit from tons of biomass originating from fruits that are discarded due to different reasons (i.e., them being overripe, crushed, or too small), from invasive seaweeds or produced as secondary products associated with tree felling, among others [28–31]. Moreover, pigment extraction from these sources could be as easy as using a suitable solvent [32–34].

DSSCs can operate indoors and under light-diffused conditions or cloudy skies. This being the case, they can be used as photovoltaic windows or integrated into greenhouses [35–38]. Additionally, applying this technology could offer an energy generation alternative, particularly for cold regions. When sensitizers are natural dyes, low temperatures constitute an ally regarding thermal stability.

Silver nanoparticles have been applied in DSSCs, increasing cell efficiency [39–41]. They enhance the electron transference towards the photoanode surface by covering bare spots on the electrode or as a part of a net with the dyes. Nanoparticles could be added mixed with the pigment as an impregnation cocktail, or by following a sequential step.

This work aimed to explore the use of anthocyanins extracted from blueberries (Southern Highbush type), primarily delphinidin-3-glucoside (Scheme 1), as sensitizers in DSSCs.

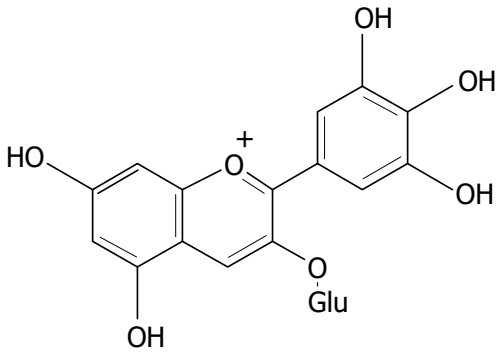

Scheme 1. Structure of delphinidin-3-glucoside (Glu = glucose).

The use of anthocyanins as sensitizers has been widely reported and constitutes one of the best options for this use among natural resources [13,42–48]. Nevertheless, exploring new sources from which to obtain these compounds and examine technological benefits could interest countries where agricultural production offers an abundant extraction origin.

For co-sensitized cells assembled with delphinidin-3-glucoside and silver round nanoparticles, we achieved a conversion efficiency of 0.24% under a power of 1 sun, AM 1.5.

2. Materials and Methods

2.1. Extraction and Purification of Dyes

Fresh samples from blueberries of the Southern Highbush type were obtained from the market. Blueberries were washed with Milli-Q water and dried at 40 °C. Two extraction options were tested: from the entire fruit or from the peel. The fruit or the peel were mechanically crushed into a mortar and mixed with liquid nitrogen. The remaining solid was dried once more at 40 °C. Then, 1 g of solid was mixed with 10 mL of solvent (Milli-Q water, acidified methanol pH = 3.5 or acidified ethanol pH = 3.5, or absolute ethanol). The mixtures were vortexed and refrigerated at 4 °C in the dark overnight. Finally, the solutions were centrifuged and the solid was discarded.

Anthocyanin extractions were followed by UV (ultraviolet)–visible spectroscopy, and the concentrations of delphinidin-3-glucoside (DEL3GLU) were calculated in accordance with Beer's law using a molar absorptivity coefficient of 29,000 L mol^{-1} cm^{-1} for the

methanol-containing solutions [49], and a coefficient of 23,700 L mol^{-1} cm^{-1} for ethanol and aqueous solutions [50].

After the extractions, the solid-free centrifuged solutions were purified via the use of C18 columns, employing an acetonitrile–methanol (ratio of 3:2) mixture as a mobile phase. The eluted solution was partially evaporated via the use of a Savant SPD 2010 Speed Vac Concentrator to increase the concentration. The purified concentrated solutions were then characterized through different techniques and applied to sensitize the DSSCs.

2.2. Characterization

FTIR spectra in the range of 400–4000 cm^{-1} were obtained at room temperature through employing a Shimadzu infrared spectrometer model IR-Prestige 21, averaging ten scans at a nominal resolution of 4 cm^{-1}. In the case of anthocyanins, a few drops of the concentrated solutions (obtained as described in Section 2.1) were deposited in a Petri dish and dried overnight. After this, the remaining solids were scratched with a spatula and thoroughly mixed with KBr in an agate mortar to obtain an approximately 1% mixture (*w*/*w*). In this way, 13 mm discs were prepared in a Pike Crush IR at a pressure of 10 tons.

Different FTIR spectra were recorded: 1—for TiO_2 (anatase form), 2—for the purified anthocyanin-containing solution (from the dried drops, as explained before), and 3—for the dye after incubation for 24 h onto TiO_2 electrodes. To obtain the dye incubate on TiO_2 samples, 100 µL of the dye-containing solutions was deposited on the FTO/TiO_2 electrodes and left at room temperature to dryness. After 24 h in darkness, a disc was prepared through the use of KBr and some milligrams of the scraped electrode surface via the described procedure.

Cyclic voltammetry was employed to evaluate the redox behavior through the use of screen-printed disposable Au-*pc* (polycrystalline) electrodes (DROPSENS) at a potential scan rate of 0.05 Vs^{-1}, with a pseudo-reference potential of E = 0.238 V vs. SHE (standard hydrogen electrode). The supporting electrolyte was ethanol/0.1 M $NaClO_4$ in milli-Q water (50/50).

For thermogravimetry (TG) and differential scanning calorimetry (DSC), 449F5 Netzsch simultaneous thermal analysis equipment was employed, using aluminum crucibles. The equipment was previously calibrated using metals as standards under heat flow and temperature. Synthetic air was used as an atmosphere with a 50 mL/min flow rate. We used a 10 °C/min heating rate. Three samples were analyzed: DEL3GLU, DEL3GLU adsorbed to TiO_2, and TiO_2. These were obtained in the same way as for FTIR, except that the DEL3GLU was obtained from a lyophilized aqueous crude extract from blueberry peels.

In addition, the stability of the DEL3GLU extracted with ethanol and water was evaluated by heating the solution at temperatures within the range of 40 to 80 °C in the presence and absence of spherical Ag nanoparticles of 100 nm (NP100). In this case, the thermal stability of the compound was followed by recording the absorbance values at 550 nm, i.e., the maximum of the visible spectra.

2.3. DSSC Assembly and Characterization

DSSCs were assembled following a sandwich configuration, with FTO/TiO_2 (SOLARONIX test kit, 20 mm × 20 mm sized, active area of mesoporous TiO_2 0.36 cm^2) and FTO/Pt (20 mm × 20 mm sized, screen printed with SOLARONIX's Pt Platinum Catalyst, as offered at the test cell kits) as the working and counter-electrodes, respectively. Both electrodes were purchased from SOLARONIX and used without further treatment. The titania opaque electrodes were printed on TCO22-7/LI glass (7 Ω/sq fluorine-doped tin oxide coating on one side), with active titania and reflective titania. The active titania was about 10 microns thick and comprised anatase nanoparticles of about 15–20 nm (porosity ~10–20 nm). The reflective titania was about 2–3 microns and composed of about 80–120 nm nanoparticles. Before use, the FTO/TiO_2 electrode was heated at 500 °C for 30 min. The electrolyte was a 50 mM iodide/tri-iodide (I^-/I_3^-) in acetonitrile (SOLARONIX Iodolyte AN-50).

Three different sensitizers were applied to assemble the DSSCs: pure ethanolic extract, pure ethanolic extract with silver nanoparticles, and aqueous crude extract.

FTO/TiO_2 electrodes were immersed overnight into the DEL3GLU-containing solution to adsorb the dye and then rinsed thoroughly with ethanol. A sequential approach was followed when silver nanoparticles were used. The dye solution was applied first, followed by the immersion of the photoanode in the nanoparticle solution [40]. Spherical Ag nanoparticles of 100 nm (NP100) (Nanocomposix®, 0.02 mg mL^{-1} of silver with 2 mmol L^{-1} of sodium citrate) were utilized.

The assembled DSSCs were characterized by measuring the current density vs. voltage (*J*–*V*) profiles and recording the electrochemical impedance spectroscopy (EIS) data with a CHI 604E potentiostat. *J*–*V* analyses were accomplished at a potential scan rate (v) of 0.05 Vs^{-1}, at room temperature, in darkness and using a solar simulator from ABET Technologies (1 sun or 100 mW cm^{-2}, AM 1.5). EIS experiments were performed between 0 and 0.5 V and inside the frequency range of 0.1 Hz to 3 MHz (in darkness).

Some additional absorbance evaluations were registered by using a reflection probe connected to a SPELEC (DROPSENS) instrument to explore the co-adsorption of anthocyanins and NP100. For this, the FTO/TiO_2 electrodes were dipped overnight inside the cocktail solutions (i.e., a mixture of purified anthocyanins and NP100) and rinsed with ethanol before being measured within the 350 to 650 nm range.

3. Results and Discussion

3.1. Extraction and Purification

As detailed in Section 2.1, different extraction conditions were applied and followed via visible spectroscopy. Concentrations were calculated accordingly to Beer's law.

The highest delphinidin-3-glucoside (DEL3GLU) contents were obtained from extractions from the whole fruit using water as an extraction solvent and from the peel using acidic methanol. For these cases, the obtained concentrations were 12×10^{-5} M. On the opposite end, the lowest delphinidin-3-glucoside amounts were obtained using ethanol as the extraction solvent starting from the peel or the whole fruit, and almost the same concentration of 2×10^{-5} M was calculated.

The absorbance spectra for the anthocyanin-containing solutions confirmed the presence of chlorophylls (peak at 666 nm) and anthocyanins (peaks at 520 and 565 nm), and therefore a C18 column was used to purify them [17,51]. Additionally, as observed in Figure 1a, the absorbance peak is very wide in ethanol, and even two superimposed peaks are detected. In neutral to slightly acidified media, anthocyanins are involved in equilibrium with their quinonoid form, and therefore two species could be seen [52–54].

Comparing the spectra recorded from the solution with those obtained from the adsorbed compounds onto the FTO/TiO_2 electrodes is interesting. Anthocyanins and chlorophylls are detected in both types of spectra (Figure 1a,b). The spectra also showed the presence of NP100 originating from the sensitizing impregnation cocktail. The ratio between the absorbance of the peak at ca. 550 nm related to the one at 666 nm changes and decreases after adsorption. This shows that chlorophylls, when present, compete with DEL3GLU for the semiconductor surface, but that their adsorption is more favorable, even in the presence of silver NP100. The presence of adsorbed NP100 could be assessed from the absorbance peaks at 380 and 420 nm due to the surface plasmon absorption band, also pointing to nanoparticle aggregation [55]. At this point, it is necessary to clarify some details. When ethanol is used to extract, chlorophylls in the raw solution are detected for the peak absorbance at 666 nm. When adsorbed to the TiO_2, they compete with the anthocyanins for the electrode surface. For this reason, chlorophylls are removed from the raw solution via the use of a C18 column to increase the cell's efficiency.

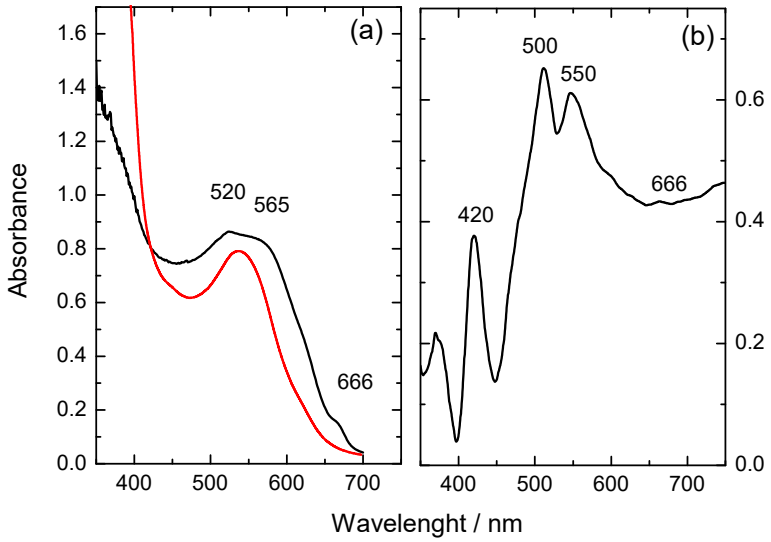

Figure 1. (**a**) Recorded visible spectra for the anthocyanin sample extracted via the use of ethanol (black line) and after purification via the use of a C18 column (red line). (**b**) Absorbance spectrum recorded using a reflection optic probe from the FTO/TiO_2 electrodes dipped overnight inside cocktail solutions prepared from anthocyanins and NP100.

3.2. FTIR

After evaporation to dryness, KBr discs were prepared to contain the purified anthocyanins and the red-colored compound after incubation for 24 h onto FTO/TiO_2 electrodes (Figure 2, Table 1). Then, those samples prepared through scratching the TiO_2 contained less DEL3GLU due to the presence of an amount of the semiconductor. Remarkably, the signals' relative intensities are irrelevant since the KBr discs were prepared through weighing 1 mg of the sample to be analyzed.

Despite this, for discs prepared from TiO_2 after incubation overnight in the anthocyanin solution, the presence of the signals assigned to DEL3GLU demonstrated the adsorption. Moreover, if the position of some of the signals moved to different frequencies, the functional group responsible for the signal was involved in the bonding with the semiconductor.

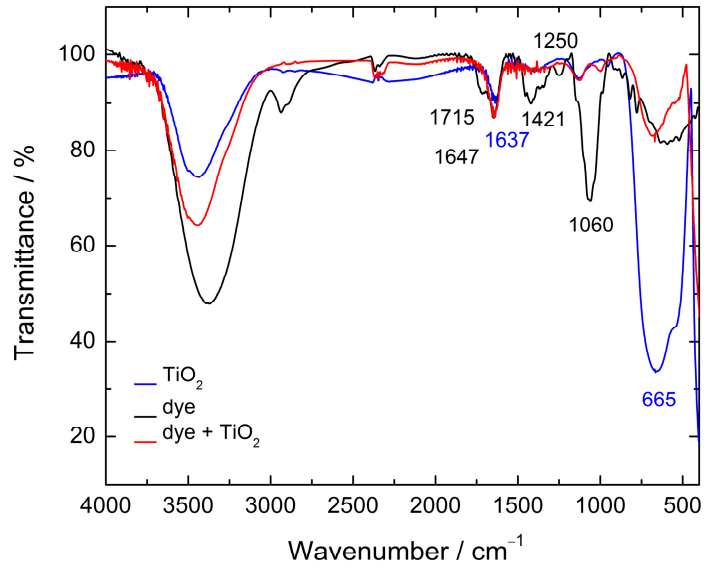

Figure 2. FTIR spectra for 1% KBr (*w*/*w*) samples. The black line corresponds to the purified DEL3GLU; the blue line to pure TiO_2 (anatase form); and the red line to the measured spectra for the dish prepared from the scraped TiO_2 sensitized with DEL3GLU.

Table 1. Main FTIR signals detected and their correspondence with the functional groups existent in the analyzed compounds.

Signal Wavenumber/cm^{-1}	Functional Group	Change after the Adsorption of DEL3GLU onto TiO_2
1715	C=O	Disappeared
1647	C=O	Moves to 1637 cm^{-1}
1454 and 1421	C-C=C phenolic	Disappeared
1250	C-O phenolic	Disappeared
1060 sharp	C-O primary alcohol C-O-C carbohydrates or flavylium	Splits in two weak signals at 1130 and 1000 cm^{-1}
665	Ti-O-Ti	Ratio between 1647/665 decreased

The double signal peak at 1715 cm^{-1} and 1647 cm^{-1} is due to C=O groups. In the TiO_2 samples, the signal at 1647 cm^{-1} detected in the dye moved to 1637 cm^{-1} after the adsorption of DEL3GLU. Establishing bonds between the dye and the semiconductor caused this displacement. To understand some details, it is important to consider the structures involved in the equilibrium. In anthocyanins, flavylium cations (red colored) and the quinonoid form (red-blue) are in equilibrium. After adsorption onto TiO_2, electrodes became red-blue colored, showing that quinonoid is the main form when conjugated to the semiconductor [31]. The quinonoid form has C=O groups, whereas the flavylium does not.

After union to the TiO_2, some signals coming from phenol groups disappeared: in particular, signals at 1454 cm^{-1} and 1421 cm^{-1} (assigned to C-C=C vibration), in addition to the signal at 1250 cm^{-1} (from C-O vibration) [56]. These observations proved that DEL3GLU could be adsorbed to the titania through using the phenolic –OH moieties.

The strong signal at 1060 cm^{-1} is split into two weak contributions at 1130 and 1000 cm^{-1} after adsorption onto TiO_2. The mentioned signal could be explained due to the C-O vibration of bonds from primary alcohol groups, such as those found in glucose and the stretching of C-O-C bonds of carbohydrates or flavylium [57,58]. These facts involved the –OH groups from glucose or the flavylium ion in coordination with titanium.

Finally, a signal related to the stretching Ti-O-Ti is detected at 665 cm^{-1}. The peak intensity at 1647 cm^{-1} ratio to the peak intensity at 665 cm^{-1} decreased after the adsorption of DEL3GLU to the semiconductor, confirming the existence of intermolecular interactions between anthocyanin and the semiconductor.

3.3. Redox Characterization

From cyclic voltammetry, profiles registered at v = 0.05 Vs^{-1} for Au-*pc* in the supporting electrolyte (ethanol/0.1 M $NaClO_4$ in Milli-Q water 50/50) displayed an anodic contribution at 0.88 V with a cathodic counter-peak at 0.52 V. The potential of the pseudo-reference electrode is 0.238 V vs. SHE. The potentials in the text are referred to as this value.

Voltametric profiles obtained for Au-*pc* in an anthocyanin solution dissolved in the supporting electrolyte showed the presence of an anodic peak at 0.98 V with a cathodic contribution at 0.52 V (Figure 3). The –OH groups from the anthocyanin adsorb to the electrode surface first, and the oxidation of this group then occurs at 0.98 V [43].

An oxidation potential of ca. 1 V is high enough to assure electronic transfer inside DSSCs once assembled through using such sensitizer in the photoelectrode.

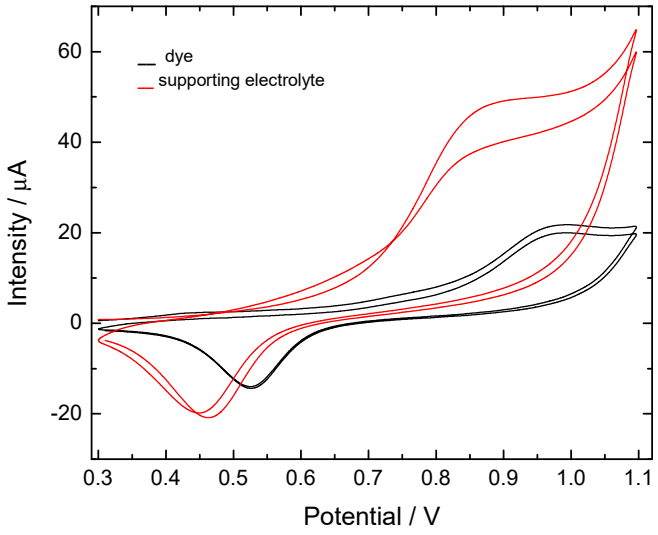

Figure 3. Voltametric profiles at v = 0.05 Vs^{-1} for Au-*pc* in the supporting electrolyte ethanol/0.1 M $NaClO_4$ in Milli-Q water 50/50 (red line) and for a DEL3GLU solution in the supporting electrolyte (black line).

3.4. Thermal Stability

The stability of DEL3GLU extracted with ethanol and water was evaluated by heating the solution at temperatures within the range of 40 to 80 °C in the presence and absence of NP100 (Figure 4). For this reason, changes in the absorption values for the maxima were recorded.

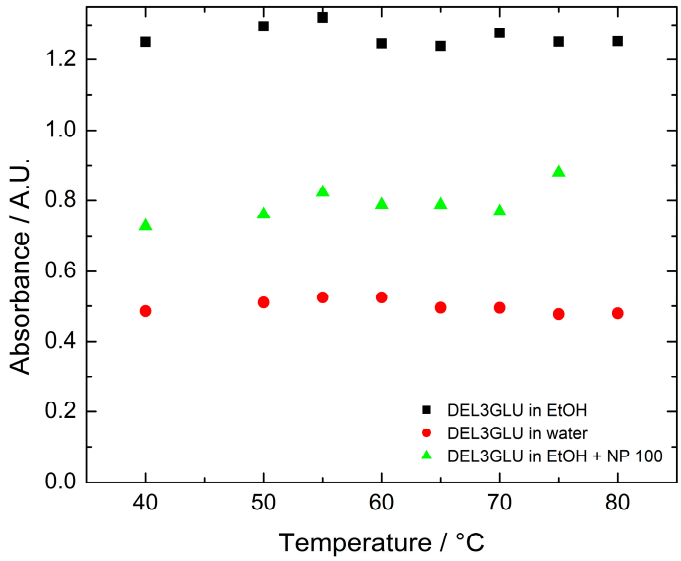

Figure 4. Thermal stability of delphinidin-3-glucoside (DEL3GLU) extracted with ethanol (black points) and water (red points), and of DEL3GLU extracted with ethanol after the addition of NP100, followed recording the absorbance values at 550 nm.

In all evaluated cases, the stability of the solutions did not show significant changes. Only a slight increase was detected at 50–55 °C and could be explained due to the co-pigmentation effect. The flavylium cation is a planar chromophore. Under the influence of the temperature, these planar structures stack with other, similar ones, resulting in increased stability instead of decomposition due to a nucleophilic attack of water, increasing the color intensity and the absorbance values [59].

3.5. TG and DSC Evaluation of the Samples

To evaluate DEL3GLU and TiO_2 adsorption, in addition to the stability of their union, TG and DSC techniques were carried out. Samples with TiO_2 were obtained from FTO/TiO_2 electrodes used to assemble the cells, and the others were used as is.

Figure 5 shows the TG and DSC thermograms. The TG signal's derivative is displayed for a better visualization of the events. From 5a, it is possible to observe weight loss during the heat treatment. Each sampling event with mass percentages and associated temperature ranges is described in Table 2. Four events were observed in the thermal decomposition of the pigment: the first, between 0 °C and 100 °C, with a mass loss of 0.5% associated with the evaporation of the solvent (water); the second, which seems to be two overlapping events (one between 100 °C and 160 °C and the other between 160 °C and 250 °C), with a 43% mass loss; the third, between 250 °C and 400 °C, with a 17% mass loss; and the fourth event, between 400 °C and 600 °C, with a 25% mass loss. Therefore, there is a 85% mass loss associated with the thermal decomposition of the pigment. Regarding TiO_2, it can be observed that there is no associated mass loss event in the range studied. While the DEL3GLU sample supported on TiO_2 shows the same type of events as DEL3GLU alone, the second and fourth events, however, are lower, as is possible to observe in the derivative thermogravimetry (DTG) plot in the inset figure and in Table 2. From Figure 5b, it is possible to observe the DSC signal for the same samples. In the TiO_2 sample, as in TG, no signal was observed. Meanwhile, for DEL3GLU it is possible to observe signals (exo and endo) in the same range of temperature indicated in the TG thermogram. In the range of 100–260 °C it is possible to distinguish a first endothermic and a second exothermic peak. In the fourth event it is possible to observe a bigger exothermic peak.

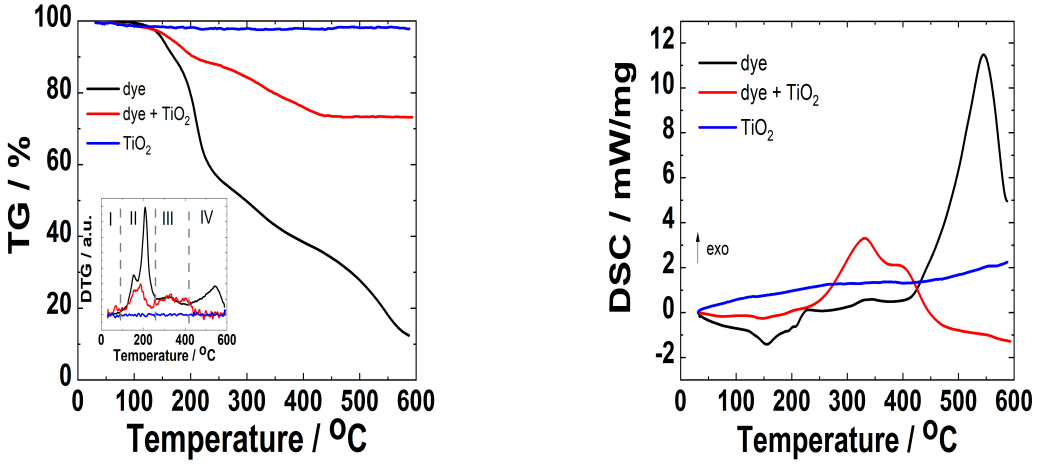

Figure 5. TG (**a**) and DSC (**b**) of different samples: purified delphinidin-3-glucoside (DEL3GLU), DEL3GLU after incubation for 24 h onto TiO_2 electrodes, and pure TiO_2 (anatase form) at a heating rate of 10 °C min. Inset: numbers I to IV denotes the events mentioned above.

Table 2. Main events raised from the TG thermograms for the analyzed samples.

Sample	Events	Nr.	Temperature Range/°C	Mass %
DEL3GLU	4	1	0–100	0.5
		2	100–160 and 160–250	43
		3	250–400	17
		4	400–600	25
DEL3GLU + TiO_2	3	1	0–100	1.3
		2	115–240	11
		3	240–450	14
TiO_2	-		-	-

Considering the structure of delphinidin-3-glucoside as a starting compound, it is possible to postulate some decomposition path. Therefore, if we take into account that, in the second event, 43% of the mass is lost, this percentage of loss could be associated with the rupture of the glycosidic bond, resulting in aglycone, which has a very unstable structure, producing the opening of the oxygenated hetero-cycle and thus losing a compound derived from delphinidin. A similar decomposition was observed in anthocyanins from black soybean, where TG and high-performance liquid chromatography (HPLC) studies were able to associate the decomposition in the range of 100 to 400 °C of sugar with the cyanin-derived molecule and its decomposition. In the last event, a loss of 25% can be observed, which would correspond to the decomposition of sugar; however, this value is slightly lower than the theoretical value (35%) [60]. This difference may be due to the difficulty of determining each reaction's start and end points since, as observed in the DTG in the range of 100 to 600 °C, there is an excellent overlapping of peaks, indicating the coexistence of decomposition reactions simultaneously. The prominent final exothermic peak observed in DSC could confirm the above, in addition to showing the difficulty in determining the start of the reaction [61,62].

Regarding the DEL3GLU supported on TiO_2, the same behavior and similar temperature ranges can be observed. Due to the difficulty of precisely knowing the proportion of anthocyanin adsorbed onto TiO_2, the observed variations in DSC and TG can be assigned to a mass effect.

3.6. DSSC Characterization

Once built up, the cells were evaluated via the recording of their *J* vs. *V* profiles and use of EIS. The results depend on the sensitizers applied: DEL3GLU or co-mixed with silver nanoparticles (Table 3, Figure 6).

Figure 6 shows the current density profiles vs. the applied potential for DSSCs sensitized with different DEL3GLU extracts or after adding silver nanoparticles sequentially. The conversion efficiency is raised in the presence of NP100; thus, a relationship between surface coverage and electron exchange can be corroborated. It is meaningful to mention that DSSCs sensitized only in the presence of NP100 reached efficiency values of 0.013%. This being the case, co-adsorption interestingly increases the measured PCE values. The best efficiency is reached when the photoanode's surface is fully covered (see an example of sensitization on Scheme 2).

Once the anthocyanins adsorb onto the FTO/TiO_2 electrode, some surface defects will remain. Using silver nanoparticles as co-sensitizers covers the remaining bare spots on the FTO/TiO_2 electrode and improves the electron transference from DEL3GLU to the semiconductor, increasing cell performance. Consequently, the current density of DSSCs is raised in the presence of NP100 [63].

Table 3. Photovoltaic properties for DCC cells assembled using different anthocyanin concentrations or extraction solvents. Measured under an intensity of 100 mW cm^{-2}, AM 1.5 G. Electrodes' active areas: 0.36 cm^2. *Jsc* is the current density, *Voc* is the open-circuit potential, *FF* is the fill factor, and η is the conversion efficiency. Results come from at least three independent experiments performed for each sensitizer. The estimated error is ± 0.005%.

	DEL3GLU in EtOH	**DEL3GLU in EtOH + NP100**	**DEL3GLU in MilliQ Water**
[ ]/M × 10^5	2.2–16.0	2.2–16.0	13.0
Jsc/mA cm^{-2}	0.51	0.71	0.33
Voc/V	0.50	0.51	0.46
FF	0.68	0.66	0.33
η/%	0.170	0.240	0.050

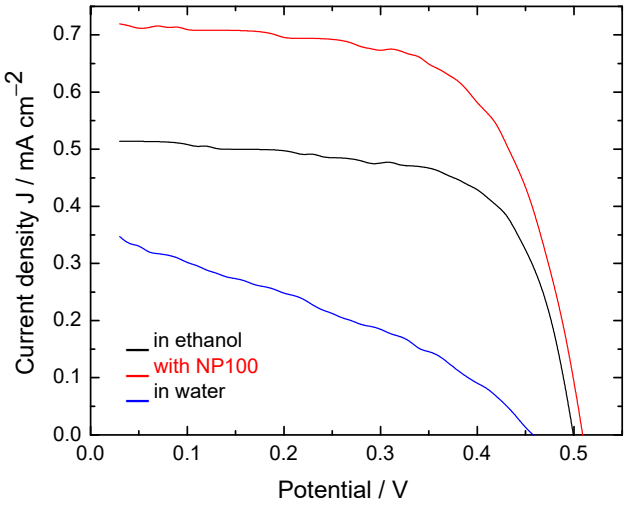

Figure 6. Photocurrent density vs. potential profiles for DSSCs under 1 sun, AM 1.5, v = 0.05 Vs^{-1}. Cells sensitized with DEL3GLU extracted with ethanol (black line), DEL3GLU extracted using Milli-Q water (blue line), and those co-sensitized using a sequential approach (DEL3GLU first extracted from ethanol and then silver nanoparticles, NP100, red line).

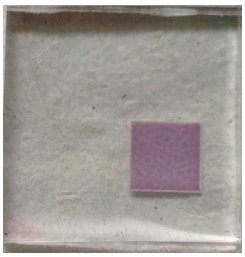

Scheme 2. Photoanode sensitized with DEL3GLU after overnight immersion in the solution.

More details about the electronic processes occurring at the DSSCs are obtained by applying EIS techniques (Figure 7). As previously reported, the impedance registers are fitted via the use of equivalent circuits integrated for several elements [64–67].

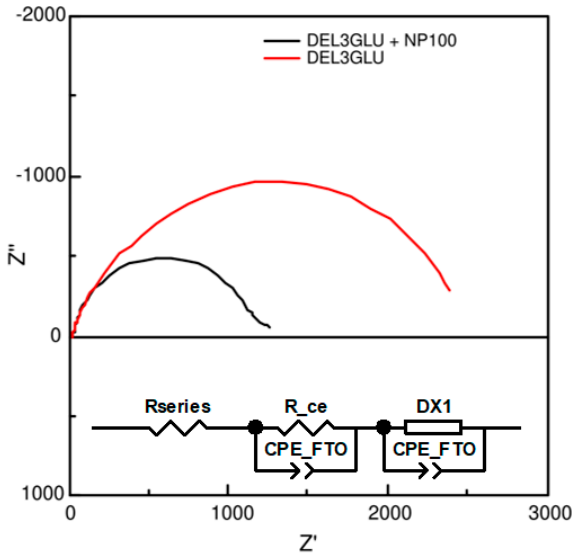

Figure 7. Nyquist representation for the impedance results measured at 0.5 V in darkness, for sensitized cells using DEL3GLU extracted with ethanol (red line), and those using DEL3GLU co-sensitized with NP100 (black line). Inset: equivalent circuit used to fit the experimental results.

Some particular parameters are useful in understanding the calculated efficiencies (displayed in Table 4):

Table 4. Determined EIS parameters for DSSCs assembled with DEL3GLU (extracted with ethanol) and also co-sensitized with NP100. Measured at 0.5 V in darkness. Results arise from at least three independent experiments performed for each sensitizer.

EIS Parameter	DEL3GLU	DEL3GLU + NP100
Rce/Ω	89	686
Ratio *Rct*/*Rt*	170	50
$\Gamma rec/s$	0.13	0.08
$\Gamma t/s$	7.7×10^{-4}	1.6×10^{-3}

Rce, the resistance associated with the regeneration of I_3^- into I^- at the counter-electrode.

Rct, the charge transport resistance for the recombination of electrons at the TiO_2/dye/electrolyte interfaces.

Rt, the electron transport resistance in the photoanode.

Γt, the time constant for the transport of the injected electrons that diffuse through the nanoparticle network. Calculated as $\Gamma t = Rt \times C\mu$ ($C\mu$, the chemical capacitance at the TiO_2/dye/electrolyte interface associated with the variation in the electron density and the displacement of the Fermi level).

Γrec, the recombination time that reflects the lifetime of an electron in the photoanode. Calculated as $\Gamma rec = Rct \times C\mu$.

Recombination implies a process of injecting electrons from the TiO_2 into the electrolyte. Then, once generated, the electrons in the dye would follow an undesired path through the mesoporous titania towards the FTO/TiO_2 interface.

High recombination times and time constants for transporting the injected electrons explain good performance efficiency.

For the analyzed samples, the electron transport times increased in the presence of the nanoparticles, affecting the cell's performance [63,68,69]. Incorporating nanoparticles improves the surface coverage; the electron mobility increases, and the electron transfer increases.

The ratio between the *Rct* and *Rt* resistances helps in understanding efficiency values. In both cases (i.e., in the presence or absence of NP100), ratios are high; thus, when electrons are generated, they follow transference across the semiconductor instead of recombining with the electrolyte.

The resistance connected to iodide regeneration at the counter-electrode (*Rce)* must also be contemplated in order to explain the calculated η values. The adsorption of molecules onto the Pt surface increases the *Rce* values. In our case, cells assembled with silver nanoparticles displayed higher *Rce* values. Once NP100 are adsorbed to the counter-electrode, the area of the electrode increases, resulting in a higher surface extent available and necessary for the I_3^- transformation into iodide; however, electron conduction through silver is worse than that through platinum, increasing *Rce*.

In summary, anthocyanins, such as delphinidin-3-glucoside, fulfill the characteristics necessary for them to be utilized as sensitizers in DSSCs, in particular, joined to silver nanoparticles.

4. Conclusions

The adsorption of delphinidin-3-glucoside extracted from blueberries (Southern Highbush type) and silver rounded nanoparticles to FTO/TiO_2 electrodes was proven from absorbance spectra recorded via the use of a reflection optic probe. FTIR measurements showed molecular interactions between the semiconductor and the delphinidin-3-glucoside through the phenolic -OH moieties of the anthocyanin. DSC and TG also confirmed the adsorption of anthocyanins to the semiconductor.

Additionally, cyclic voltametric measurements showed an anodic contribution at 0.98 V raised from the oxidation of -OH groups of the delphinidin-3-glucoside, enough to assure the electronic transfer inside DSSCs via the use of a sensitizer in the photoelectrode. Additionally, regarding its application as a light harvester in a device exposed to the sun and, therefore, its capacity to warm up, the stability of delphinidin-3-glucoside was evaluated by heating the solutions to 80 °C without any significant change.

Once assembled in DSSCs, the photoelectrodes sensitized with delphinidin or co-sensitized with nanoparticles showed high recombination times and time constants for transporting the injected electrons; however, power conversion efficiencies were higher in the presence of NP100, probably due to obtaining a better surface coverage.

The exposed results indicated the possibility of applying delphinidin-3-glucoside extracted from blueberries following a straightforward path as potential impregnation dyes in DSSCs, particularly in the presence of co-adsorbents, such as silver nanoparticles, offering a technological application of discarded and not commercialized fruits for countries where agricultural production provides an abundant origin of extraction.

Author Contributions: Conceptualization, methodology, supervision, formal analysis, preparation, and writing—original draft, review, and editing, M.F.C.; investigation, formal analysis, and writing—original draft, T.M.; formal analysis and writing—original draft, M.R.C. All authors have read and agreed to the published version of the manuscript.

Funding: This research received no external funding.

Institutional Review Board Statement: Not applicable.

Informed Consent Statement: Not applicable.

Data Availability Statement: Not applicable.

Acknowledgments: M.F.C. and M.R. are ANII (Agencia Nacional de Investigación e Innovación) and PEDECIBA (Programa de Desarrollo de las Ciencias Básicas) researchers.

Conflicts of Interest: The authors declare no conflict of interest.

References

1. Bisquert, J.; Cahen, D.; Hodes, G.; Rühle, S.; Zaban, A. Physical Chemical Principles of Photovoltaic Conversion with Nanoparticulate, Mesoporous Dye-Sensitized Solar Cells. *J. Phys. Chem. B* **2004**, *108*, 8106–8118. [CrossRef]
2. Muñoz-García, A.B.; Benesperi, I.; Boschloo, G.; Concepcion, J.J.; Delcamp, J.H.; Gibson, E.A.; Meyer, G.J.; Pavone, M.; Pettersson, H.; Hagfeldt, A.; et al. Dye-sensitized solar cells strike back. *Chem. Soc. Rev.* **2021**, *50*, 12450–12550. [CrossRef] [PubMed]
3. Yella, A.; Lee, H.W.; Tsao, H.N.; Yi, C.; Chandiran, A.K.; Nazeeruddin, M.K.; Diau, E.W.G.; Yeh, C.Y.; Zakeeruddin, S.M.; Grätzel, M. Porphyrin-sensitized solar cells with cobalt (II/III)-based redox electrolyte exceed 12 percent efficiency. *Science* **2011**, *334*, 629–634. [CrossRef]
4. Mahalingam, S.; Manap, A.; Lau, K.S.; Omar, A.; Chelvanathan, P.; Chia, C.H.; Amin, N.; Mathews, I.J.; Afandi, N.F.; Rahim, N.A. Mixture deposition method for graphene quantum dots-based dye-sensitized solar cell. *Electrochim. Acta* **2022**, *404*, 139732. [CrossRef]
5. Mahalingam, S.; Nugroho, A.; Floresyona, D.; Lau, K.S.; Manap, A.; Chia, C.H.; Afandi, N. Bio and non bio materials based quasi solid state electrolytes in DSSC: A review. *Int. J. Energy Res.* **2022**, *46*, 5399–5422. [CrossRef]
6. Mahalingam, S.; Manap, A.; Rabeya, R.; Lau, K.S.; Chia, C.H.; Abdullah, H.; Amin, N.; Chelvanathan, P. Electron transport of chemically treated graphene quantum dots-based dye-sensitized solar cells. *Electrochim. Acta* **2023**, *439*, 141667. [CrossRef]
7. Syrrokostas, G.; Leftheriotis, G.; Yannopoulos, S.N. Lessons learned from 25 years of development of photoelectrochromic devices: A technical review. *Renew. Sustain. Energy Rev.* **2022**, *162*, 112462. [CrossRef]
8. O'Regan, B.; Grätzel, M. A low-cost, high-efficiency solar cell based on dye-sensitized colloidal TiO_2 films. *Nature* **1991**, *353*, 737–740. [CrossRef]
9. Chang, H.; Wu, H.M.; Chen, T.L.; Huang, K.D.; Jwo, C.S.; Lo, Y.J. Dye-sensitized solar cell using natural dyes extracted from spinach and ipomoea. *J. Alloys Compd.* **2010**, *495*, 606–610. [CrossRef]
10. Wang, X.-F.; Matsuda, A.; Koyama, Y.; Nagae, H.; Sasaki, S.; Tamiaki, H.; Wada, Y. Effects of plant carotenoid spacers on the performance of a dye-sensitized solar cell using a chlorophyll derivative: Enhancement of photocurrent determined by one electron-oxidation potential of each carotenoid. *Chem. Phys. Lett.* **2006**, *423*, 470–475. [CrossRef]

11. Zhang, D.; Stojanovic, M.; Ren, Y.; Cao, Y.; Eickemeyer, F.T.; Socie, E.; Vlachopoulos, N.; Moser, J.-E.; Zakeeruddin, S.M.; Hagfeldt, A.; et al. A molecular photosensitizer achieves a Voc of 1.24 V enabling highly efficient and stable dye-sensitized solar cells with copper(II/I)-based electrolyte. *Nat. Commun.* **2021**, *12*, 1777. [CrossRef] [PubMed]
12. Ghann, W.; Kang, H.; Sheikh, T.; Yadav, S.; Chavez-Gil, T.; Nesbitt, F.; Uddin, J. Fabrication, Optimization and Characterization of Natural Dye Sensitized Solar Cell. *Sci. Rep.* **2017**, *7*, 41470. [CrossRef] [PubMed]
13. Calogero, G.; Bartolotta, A.; DiMarco, G.; Di Carlo, A.; Bonaccorso, F. Vegetable-based dye-sensitized solar cells. *Chem. Soc. Rev.* **2015**, *44*, 3244–3294. [CrossRef] [PubMed]
14. Zhou, H.; Wu, L.; Gao, Y.; Ma, T. Dye-sensitized solar cells using 20 natural dyes as sensitizers. *J. Photochem. Photobiol. A Chem.* **2011**, *219*, 188–194. [CrossRef]
15. Singh, S.; Maurya, I.C.; Sharma, S.; Kushwaha, S.P.S.; Srivastava, P.; Bahadur, L. Application of new natural dyes extracted from Nasturtium flowers (Tropaeolum majus) as photosensitizer in dye-sensitized solar cells. *Optik* **2021**, *243*, 167331. [CrossRef]
16. Concepcion, R.; Alejandrino, J.; Mendigoria, C.H.; Dadios, E.; Bandala, A.; Sybingco, E.; Vicerra, R.R. Lactuca sativa leaf extract concentration optimization using evolutionary strategy as photosensitizer for TiO_2-filmed Grätzel cell. *Optik* **2021**, *242*, 166931. [CrossRef]
17. Hernández-Martínez, A.R.; Estevez, M.; Vargas, S.; Quintanilla, F.; Rodríguez, R. Natural Pigment-Based Dye-Sensitized Solar Cells. *J. Appl. Res. Technol.* **2012**, *38*, 38–47. [CrossRef]
18. Bekele, E.T.; Sintayehu, Y.D. Recent Progress, Advancements, and Efficiency Improvement Techniques of Natural Plant Pigment-Based Photosensitizers for Dye-Sensitized Solar Cells. *J. Nanomat.* **2022**, *2022*, 1024100. [CrossRef]
19. Pinto, A.L.; Cruz, H.; Oliveira, J.; Araújo, P.; Cruz, L.; Gomes, V.; Silva, C.P.; Silva, G.T.M.; Mateus, T.; Calogero, G.; et al. Dye-sensitized solar cells based on dimethylamino-π-bridgepyrano anthocyanin dyes. *Sol. Energy* **2020**, *206*, 188–199. [CrossRef]
20. Barichello, J.; Mariani, P.; Matteocci, F.; Vesce, L.; Reale, A.; Di Carlo, A.; Lanza, M.; Di Marco, G.; Polizzi, S.; Calogero, G. The Golden Fig: A Plasmonic Effect Study of Organic-Based Solar Cells. *Nanomaterials* **2022**, *12*, 267. [CrossRef]
21. Golshan, M.; Osfouri, S.; Azin, R.; Jalali, T.; Moheimani, N.R. Co-sensitization of natural and low-cost dyes for efficient panchromatic light-harvesting using dye-sensitized solar cells. *J. Photochem. Photobiol. A Chem.* **2021**, *417*, 113345–113356. [CrossRef]
22. Orona-Navar, A.; Aguilar-Hernandez, I.; Nigam, K.D.P.; Cerdan-Pasar, A.; Ornelas-Soto, N. Alternative sources of natural pigments for dye-sensitized solar cells: Algae, cyanobacteria, bacteria, archaea and fungi. *J. Biotechnol.* **2021**, *332*, 29–53. [CrossRef] [PubMed]
23. Amogne, N.Y.; Ayele, D.W.; Tsigie, Y.A. Recent advances in anthocyanin dyes extracted from plants for dye sensitized solar cell. *Mater. Renew. Sustain. Energy* **2020**, *9*, 23–39. [CrossRef]
24. Leite, A.M.B.; da Cunha, H.O.; Rodrigues, J.A.F.C.R.R.; Babu, S.; de Barros, A.L.F. Construction and characterization of organic photovoltaic cells sensitized by Chrysanthemum based natural dye. *Spectrochim. Acta A Mol. Biomol. Spectrosc.* **2023**, *284*, 121780–121788. [CrossRef]
25. Prakash, P.; Balasundaram, J.; Al-Enizi, A.M.; Ubaidullah, M.; Pandit, B. Effect of photovoltaic performance of plant-based cocktail DSSCs and adsorption of nano TiO_2 onto the solvent-influenced dye sensitizers. *Opt. Mater.* **2022**, *133*, 113031–113040. [CrossRef]
26. Bist, A.; Chatterjee, S. Review on Efficiency Enhancement Using Natural Extract Mediated Dye-Sensitized Solar Cell for Sustainable Photovoltaics. *Energy Technol.* **2021**, *9*, 2001058–2001077. [CrossRef]
27. Cho, K.-C.; Chang, H.; Chen, C.-H.; Kao, M.-J.; Lai, X.-R. A Study of Mixed Vegetable Dyes with Different Extraction Concentrations for Use as a Sensitizer for Dye-Sensitized Solar Cells. *Int. J. Photoenergy* **2014**, *2014*, 492747. [CrossRef]
28. Pereira, A.G.; Fraga-Corral, M.; Garcia-Oliveira, P.; Lourenço-Lopes, C.; Carpena, M.; Prieto, M.A.; Simal-Gandara, J. The Use of Invasive Algae Species as a Source of Secondary Metabolites and Biological Activities: Spain as Case-Study. *Mar. Drugs* **2021**, *19*, 178. [CrossRef]
29. Milledge, J.; Nielsen, B.; Bailey, D. High-value products from macroalgae: The potential uses of the invasive brown seaweed, Sargassum muticum. *Rev. Environ. Sci. Bio/Technol.* **2016**, *15*, 67–88. [CrossRef]
30. Sankaranarayanan, S.; Kathiravan, I.; Balasundaram, J. An analysis of the dye-sensitized solar cells fabricated with the dyes extracted from the leaves and flowers of Amaranthus cruentus. *Environ. Sci. Pollut. Res.* **2022**, *29*, 44271–44281. [CrossRef]
31. Vardan, M.K.; Garg, S. Performance of Dye-Sensitized Solar Cell using Hamelia Patens leaves as natural dye. *IOP Conf. Ser. Mater. Sci. Eng.* **2022**, *1248*, 012105. [CrossRef]
32. Parisi, M.L.; Sinicropi, A.; Basosi, R. Life cycle assessment of Graetzel-type cell production for non conventional photovoltaics from novel organic dyes. *Int. J. Heat Technol.* **2011**, *29*, 161.
33. Shanmugam, V.; Manoharan, S.; Sharafali, A.; Anandan, S.; Murugan, R. Green grasses as light harvesters in dye sensitized solar cells. *Spectrochim. Acta A Mol. Biomol. Spectros.* **2015**, *135*, 947–952. [CrossRef] [PubMed]
34. Lim, A.; Haji-Manaf, N.; Tennakoon, K.; Chandrakanthi, R.L.; Lim, L.B.; Bandara, J.M.; Ekanayake, P. Higher Performance of DSSC with Dyes from *Cladophora* sp. as Mixed Cosensitizer through Synergistic Effect. *J. Biophys.* **2015**, *2015*, 510467. [CrossRef] [PubMed]
35. Shanmugapriya, T.; Balavijayalakshmi, J. Efficiency Studies of Galinsoga Parviflora Pigments as a Sensitizer in Pt Free Graphene Oxide/Nickel Oxide Counter Electrode: Dye Sensitized Solar Cell Applications. *J. Clust. Sci.* **2021**, *32*, 1277–1288. [CrossRef]

36. Mariotti, B.N.; Gerbaldi, C.; Bonomo, M.; Bella, F.; Fagiolari, L.; Barbero, N.; Barolo, C. Recent advances in eco-friendly and cost-effective materials towards sustainable dye-sensitized solar cells. *Green Chem.* **2020**, *22*, 7168–7218. [CrossRef]
37. Parisi, M.L.; Maranghi, S.; Basosi, R. The evolution of the dye sensitized solar cells from Grätzel prototype to up-scaled solar applications: A life cycle assessment approach. *Renew. Sustain. Energy Rev.* **2014**, *39*, 124–138. [CrossRef]
38. Ursu, D.; Vajda, M.; Miclau, M. Highly efficient dye-sensitized solar cells for wavelength-selective greenhouse: A promising agrivoltaic system. *Int. J. Energy Res.* **2022**, *46*, 18550–18561. [CrossRef]
39. Dissanayake, A.K.L.; Kumari, J.M.K.; Senadeera, G.K.R.; Thotawatthage, C.A. Efficiency enhancement in plasmonic dye-sensitized solar cells with TiO_2 photoanodes incorporating gold and silver nanoparticles. *J. Appl. Electrochem.* **2016**, *46*, 47–58. [CrossRef]
40. Cerdá, M.F.; Botasini, S. Co-sensitized cells from Antarctic resources using Ag nanoparticles. *Surf. Interface Anal.* **2020**, *52*, 980–984. [CrossRef]
41. Saravanan, S.; Kato, R.; Balamurugan, M.; Kaushik, S.; Soga, T. Efficiency improvement in dye sensitized solar cells by the plasmonic effect of green synthesized silver nanoparticles. *J. Sci. Adv. Mater. Devices* **2017**, *2*, 418–424. [CrossRef]
42. Lucioli, S.; Di Bari, C.; Forni, C.; Di Carlo, A.; Barrajón-Catalán, E.; Micol, V.; Nota, P.; Teoli, F.; Matteocci, F.; Frattarelli, A.; et al. Anthocyanic pigments from elicited in vitro grown shoot cultures of Vaccinium corymbosum L., cv. Brigitta Blue, as photosensitizer in natural dye-sensitized solar cells (NDSSC). *J. Photochem. Photobiol. B Biol.* **2018**, *188*, 69–76. [CrossRef] [PubMed]
43. Enciso, P.; Decoppet, J.D.; Grätzel, M.; Wörner, M.; Cabrerizo, F.M.; Cerdá, M.F. A cockspur for the DSS cells: Erythrina crista-galli sensitizers. *Spectrochim. Acta A Mol. Biomol. Spectros.* **2017**, *176*, 91–98. [CrossRef] [PubMed]
44. Calogero, G.; Di Marco, G. Red Sicilian orange and purple eggplant fruits as natural sensitizers for dye-sensitized solar cells. *Sol. Energy Mater Sol. Cells* **2008**, *92*, 1341–1346. [CrossRef]
45. Pinto, A.L.; Oliveira, J.; Araújo, P.; Calogero, G.; de Freitas, V.; Pina, F.; Parola, A.J.; Lima, J.C. Study of the multi-equilibria of red wine colorants pyranoanthocyanins and evaluation of their potential in dye-sensitized solar cells. *Sol. Energy* **2019**, *191*, 100–108. [CrossRef]
46. Calogero, G.; Citro, I.; Crupi, C.; Carini, G.; Arigò, D.; Spinella, G.; Bartolotta, A.; Di Marco, G. Absorption spectra, thermal analysis, photoelectrochemical characterization and stability test of vegetable-based dye-sensitized solar cells. *Opt. Mater.* **2019**, *88*, 24–29. [CrossRef]
47. Teoli, F.; Lucioli, S.; Nota, P.; Frattarelli, A.; Matteocci, F.; Di Carlo, A.; Caboni, E.; Forni, C. Role of pH and pigment concentration for natural dye-sensitized solar cells treated with anthocyanin extracts of common fruits. *J. Photochem. Photobiol. A Chem.* **2016**, *316*, 24–30. [CrossRef]
48. González Steffano, M.; Alvarez, E.; Sosa, P.; Vázquez, C.; Cerdá, M.F. Pitanga anthocyanins as sensitizers for DSSC. *Innotec* **2022**, *23*, e584. [CrossRef]
49. Santiago, M.C.P.d.A.; Gouvêa, A.C.M.S.; Godoy, R.L.d.O.; Borguini, R.G.; Pacheco, S.; Nogueira, R.I.; Nascimento, L.d.S.d.M.; Freitas, S.P. Analytical standards production for the analysis of pomegranate anthocyanins by HPLC. *Braz. J. Food Technol.* **2014**, *17*, 51–57. [CrossRef]
50. Kähkönen, M.P.; Heinämäki, J.; Ollilainen, V.; Heinonen, M. Berry anthocyanins: Isolation, identification and antioxidant activities. *J. Sci. Food Agric.* **2003**, *83*, 1403–1411. [CrossRef]
51. Yazie, N.; Ayele, D.; Woldu, A. Natural dye as Light-Harvesting pigments for Quasi-Solid-State Dye-Sensitized solar cells. *Mater. Renew. Sustain. Energy* **2016**, *5*, 13. [CrossRef]
52. Escobar, M.A.M.; Jaramillo, F. Thermally and UV Stable Natural Dyes with Potential Use in Efficient Photoelectrochemical Devices. *J. Renew. Mater.* **2015**, *3*, 302–317. [CrossRef]
53. Abdel-Aal, E.-S.M.; Hucl, P. A Rapid Method for Quantifying Total Anthocyanins in Blue Aleurone and Purple Pericarp Wheats. *Cereal Chem.* **1999**, *76*, 350–354. [CrossRef]
54. Welch, C.R.; Wu, Q.; Simon, J.E. Recent Advances in Anthocyanin Analysis and Characterization. *Curr. Anal. Chem.* **2008**, *4*, 75–101. [CrossRef] [PubMed]
55. Bastús, N.G.; Merkoçi, F.; Piella, J.; Puntes, V. Synthesis of Highly Monodisperse Citrate-Stabilized Silver Nanoparticles of up to 200 nm: Kinetic Control and Catalytic Properties. *Chem. Mater.* **2014**, *26*, 2836–2846. [CrossRef]
56. Agatonovic-Kustrin, S.; Morton, D.W.; Yusof, A.P.M. The Use of Fourier Transform Infrared (FTIR) Spectroscopy and Artificial Neural Networks (ANNs) to Assess Wine Quality. *Mod. Chem. Appl.* **2013**, *1*, 4. [CrossRef]
57. Favaro, L.; Balcão, V.; Rocha, L.; Silva, E.; Oliveira, J., Jr.; Vila, M.; Tubino, M. Physicochemical Characterization of a Crude Anthocyanin Extract from the Fruits of Jussara (Euterpe edulis Martius): Potential for Food and Pharmaceutical Applications. *J. Braz. Chem. Soc.* **2018**, *29*, 2072–2088. [CrossRef]
58. Bu, C.; Zhang, Q.; Zeng, J.; Cao, X.; Hao, Z.; Qiao, D.; Xu, H.; Cao, Y. Identification of novel anthocyanins synthesis pathway from fungus, Aspergillus sydowii H-1. *BMC Genomics* **2020**, *21*, 29. [CrossRef]
59. Horbowicz, M.; Kosson, R.; Grzesiuk, A.; Dębski, H. Anthocyanins of Fruits and Vegetables—Their Occurrence, Analysis and Role in Human Nutrition. *J. Fruit Ornam. Plant Res.* **2008**, *68*, 5–22. [CrossRef]
60. Wang, D.; Ma, Y.; Zhang, C.; Zhao, X. Thermal characterization of the anthocyanins from black soybean (Glycine max L.) exposed to thermogravimetry. *LWT—Food Sci. Technol.* **2014**, *55*, 645–649. [CrossRef]
61. Silva Dos Passos, A.P.; Madrona, G.S.; Marcolino, V.A.; Baesso, M.L.; Matioli, G. The Use of Thermal Analysis and Photoacoustic Spectroscopy in the Evaluation of Maltodextrin Microencapsulation of Anthocyanins from Juçara Palm Fruit (Euterpe edulis Mart.) and Their Application in Food. *Food Technol. Biotechnol.* **2015**, *53*, 385–396. [CrossRef] [PubMed]

62. Osorio, C.; Acevedo, B.; Hillebrand, S.; Carriazo, J.; Winterhalter, P.; Morales, A.L. Microencapsulation by Spray-Drying of Anthocyanin Pigments from Corozo (Bactris guineensis) Fruit. *J. Agric. Food Chem.* **2010**, *58*, 6977–6985. [CrossRef] [PubMed]
63. Borbon, S.; Lugo, S.; Pourjafari, D.; Pineda Aguilar, N.; Oskam, G.; Lopez, I. Open-Circuit Voltage (VOC) Enhancement in TiO_2-Based DSSCs: Incorporation of ZnO Nanoflowers and Au Nanoparticles. *ACS Omega* **2020**, *5*, 10977–109986. [CrossRef] [PubMed]
64. Marizcurrena, J.J.; Castro-Sowinski, S.; Cerdá, M.F. Improving the performance of dye-sensitized solar cells using nanoparticles and a dye produced by an Antarctic bacterium. *Environ. Sustain.* **2021**, *4*, 711–721. [CrossRef]
65. Yañuk, J.G.; Cabrerizo, F.M.; Dellatorre, F.G.; Cerdá, M.F. Photosensitizing role of R-phycoerythrin red protein and β-carboline alkaloids in Dye sensitized solar cell. Electrochemical and spectroscopic characterization. *Energy Rep.* **2020**, *6*, 25–36. [CrossRef]
66. Montagni, T.; Enciso, P.; Marizcurrena, J.J.; Castro-Sowinski, S.; Fontana, C.; Davyt, D.; Cerdá, M.F. Dye sensitized solar cells based on Antarctic Hymenobacter sp. UV11 dyes. *Environ. Sustain.* **2018**, *1*, 89–97. [CrossRef]
67. Bisquert, J. Theory of the impedance of charge transfer via surface states in dye-sensitized solar cells. *J. Electroanal. Chem.* **2010**, *646*, 43–51. [CrossRef]
68. Chowdhury, F.I.; Buraidah, M.H.; Arof, A.K.; Mellander, B.E.; Noor, I.M. Impact of tetrabutylammonium, iodide and triiodide ions conductivity in polyacrylonitrile based electrolyte on DSSC performance. *Sol. Energy* **2020**, *196*, 379–388. [CrossRef]
69. Lana-Villarreal, T.; Boschloo, G.; Hagfeldt, G.A. Nanostructured Zinc Stannate as Semiconductor Working Electrodes for Dye-Sensitized Solar Cells. *J. Phys. Chem. C* **2007**, *111*, 5549–5556. [CrossRef]